Proceedings World Geothermal Congress 2026
Calgary, Canada, June 8 – 11, 2026

Heat transfer characterizations of supercritical CO_2 flow through a rough fracture in the Hot Dry Rock

Jiawei Li[1,2], Hongyang Meng[1,2], Gensheng Li[3], Xianzhi Song[3*], Le Zhang[1,4], Jichao Fang[1,4], Xiaoli Huang[5]

[1], State Key Laboratory of Deep Geothermal Enrichment Mechanisms and Efficient Development, Beijing, 100083, China

[2], School of Mechanical and Transportation Engineering, China University of Petroleum (Beijing), 102249, China

[3], State Key Laboratory of Petroleum Resources and Engineering, China University of Petroleum (Beijing), Beijing,102249, China

[4], Petroleum Exploration and Production Research Institute, SINOPEC, Beijing, 102206, China

[5], School of Engineering, North China Electric Power University, Beijing, 102206, China

Corresponding E-mail Address: songxz@cup.edu.cn

Keywords: Supercritical CO_2, Enhanced Geothermal Systems, Rough fractures, Heat Production Rate, Multi-objective Optimization

ABSTRACT

With the global energy structure transitioning toward low-carbonization, Enhanced Geothermal Systems (EGS) as a key technology for efficient development of hot dry rock resources has attracted significant attention. Supercritical carbon dioxide (sCO_2), due to its low viscosity, high diffusivity, and synergistic carbon sequestration potential, has emerged as a highly promising alternative working fluid. This study focuses on the flow and heat transfer characteristics of sCO_2 in geothermal fractures. Based on fractal dimension theory, an irregular fracture model was constructed, and combined with computational fluid dynamics (CFD) methods, the effects of fracture surface temperature, injection parameters, ambient pressure, and anisotropy factor on sCO_2 flow and heat transfer were systematically analyzed. The results show that sCO_2 exhibits significant non-Darcy flow characteristics in fractal fractures; abrupt changes in physical properties near the critical point lead to flow instability, necessitating optimization of injection pressure to avoid local thermal efficiency degradation; when fracture surface temperature, injection temperature, injection flow rate, ambient pressure, and anisotropy factor change, the flow and heat transfer characteristics of sCO_2 change regularly. The variation law of heat production rate is closely related to flow and heat transfer characteristics, which can intuitively reflect heat exchange efficiency under different conditions. This research provides a theoretical basis for the engineering design and operational optimization of sCO_2-EGS, and is of great significance for promoting the development of integrated geothermal-carbon sequestration technology.

1 INTRODUCTION

Geothermal energy, as a clean and renewable energy source, holds significant importance in alleviating the energy crisis and reducing environmental pollution. It is also one of the core baseload energy sources for replacing fossil fuels under the global carbon neutrality goal [1]. According to predictions by the International Energy Agency (IEA), geothermal power generation needs to reach 1400 TW·h by 2050 to meet emission reduction requirements [2]. However, traditional Enhanced Geothermal Systems (EGS), which use water as their working fluid, face three major bottlenecks: high consumption of water resources, making them unsuitable for arid regions; a tendency to cause equipment scaling and significant mechanical erosion of production wells; and a high risk of inducing seismicity.

Supercritical carbon dioxide (sCO_2) possesses unique physical properties, such as a density similar to liquids, viscosity close to gases, and a high diffusion coefficient. These properties not only enhance heat transfer efficiency and fluid mobility but also enable simultaneous carbon sequestration, offering a potential optimization path for geothermal extraction [3]. Currently, research on the flow and heat transfer characteristics of sCO_2 under conditions of strongly variable thermophysical properties in geothermal fractures, as well as the interaction mechanisms with fracture surfaces, remains relatively limited, hindering further technological development [4]. Therefore, conducting research under high-temperature and high-pressure conditions holds significant theoretical and practical importance.

International scholars have conducted extensive studies, proposing equations of state such as the Peng-Robinson equation [5] and cubic equations like Soave-Redlich-Kwong [6] to describe the physical properties of sCO_2. Magliocco et al. experimentally investigated the flow and heat transfer characteristics of sCO_2 in porous

media, providing a basis for the development of EGS [7]. Domestically, Zhang Le's team monitored fracture wall temperature, fluid temperature, and the dynamic variation of net heat to study the flow and heat transfer characteristics in smooth granite fractures, determining the Nusselt number. They discovered that the thermal conductivity of sCO_2 peaks near the critical point and that the mass flow rate is significantly correlated with heat transfer efficiency [8]. Gong Liang's team pointed out that hot dry rock reservoirs are dense and have low permeability, requiring the construction of complex fracture networks through hydraulic fracturing to enhance permeability [9]. Han Dongxu's team confirmed that fracture geometric parameters and wall temperature distribution significantly influence the flow and heat transfer of sCO_2, and that the thermophysical parameters of the injected fluid need to be treated as variables in reservoir heat extraction analysis [10].

Regarding the flow and heat transfer characteristics of supercritical carbon dioxide in geothermal reservoirs, international scholars have conducted numerous laboratory and field experimental studies. Zhang et al. compared H_2O-EGS and CO_2-EGS systems, confirming the significant advantages of CO_2-EGS in thermal energy extraction and achieving the synergy of "heat extraction and carbon sequestration" [11]. Brown's pioneering theory demonstrated that replacing water with sCO_2 (at the critical state of 31.1°C and 7.38 MPa) can reduce carbon emissions, lower circulation energy consumption, and mitigate equipment corrosion. Furthermore, reactions between rock minerals, CO_2, and water can achieve permanent carbon sequestration [12]. Remoroza et al. further validated the suitability of CO_2 as a working fluid, noting that its low viscosity, high compressibility, and other characteristics can reduce flow resistance and create a self-driving force [13].

Numerical simulation is an important method for studying the flow and heat transfer characteristics of supercritical carbon dioxide in geothermal extraction fractures. Li Shuai's team used fractal interpolation and the Monte Carlo method to construct models, analyzing the effects of geothermal parameters such as injection temperature and pressure difference on seepage and thermal extraction performance [14]. Xu Zhihao's team found that CO_2 fracturing fluid undergoes phase transition to a supercritical state through heat exchange after injection into the formation, and a temperature gradient forms in the formation [15]. Jiang Haiyang et al. established a discrete fracture network model, providing a model reference for related research [16]. Wang et al. used molecular simulation to analyze the effects of temperature and pore size on the flow velocity of supercritical octane [17]. Jiang et al. investigated the influence of pore scale on the transport of supercritical methane [18]. International scholars have also utilized software such as COMSOL Multiphysics and ANSYS Fluent for modeling. For example, Yao et al. established a three-dimensional thermal-hydraulic-mechanical coupling model based on the Discrete Fracture Model (DFM), using the Desert Peak EGS project as a case study to optimize engineering design [19].

This project will comprehensively employ numerical simulation and theoretical analysis methods to conduct an in-depth study of the flow and heat transfer characteristics of supercritical carbon dioxide in geothermal extraction fractures. The numerical simulation research aims to analyze the flow and heat transfer behavior of carbon dioxide under complex geological conditions, providing support for the optimization of extraction schemes. The theoretical analysis will focus on revealing the interaction mechanisms between carbon dioxide and fracture surfaces, laying a theoretical foundation for establishing accurate convective heat transfer models.

2 MATHEMATICAL MODELLING

Based on fractal dimension theory, this study constructs an irregular fracture model and combines computational fluid dynamics methods to systematically analyze the effects of ambient pressure, injection flow rate, injection temperature, and wall temperature on the flow and heat transfer characteristics and the heat production rate of supercritical carbon dioxide.

2.1 Governing Equations

Continuity equation:

$$\frac{\partial \rho_f}{\partial t} + \nabla \cdot (\rho_f)\vec{v} \tag{1}$$

Momentum equation:

$$\frac{\partial (\rho_f \vec{v})}{\partial t} + \nabla \cdot (\rho_f \vec{v}\vec{v}) = -\nabla p + \nabla \cdot (\mu_f [(\nabla \vec{v} + \nabla \vec{v}^T) - \frac{2}{3} \cdot \nabla \vec{v}\, \text{I}\!\text{I}\,]) \tag{2}$$

Energy equation:

$$\frac{\partial(\rho_f E)}{\partial t} + \nabla \cdot \left(\vec{v}\left(\rho_f E + p\right)\right) = \nabla \cdot \left(\lambda_f \nabla T + \mu \left[(\nabla \vec{v} + \nabla \vec{v}^T) - \frac{2}{3} \cdot \nabla \vec{v}\, \mathrm{II}\right] \cdot \vec{v}\right) \quad (3)$$

The variation pattern of the supercritical carbon dioxide fluid temperature can be theoretically analyzed through the energy equation to examine the process of heat transfer and conversion [20].

2.2 Model Establishment

A model with a side length of 5 cm was established. This dimension was selected because the actual rock cores extracted in geological operations typically range from one to four inches (2.54–10.16 cm) [21]. A uniformly divided grid was applied in the x and y directions, while in the z direction, random heights were generated characterized by a fractal dimension. Roughness features at different scales, i.e., the fracture surfaces, were superimposed via Gaussian distribution. Fractal dimension is commonly used to describe complex surfaces; a larger fractal dimension corresponds to a higher degree of surface roughness, which also serves to differentiate it from flow and heat transfer over smooth walls. Python code was utilized to generate a fractal height field, export the height data, and import the CSV file into software to define the z-coordinates of the fracture surfaces. The anisotropy factor was set to 1 and 1.05. When the anisotropy factor is greater than 1, the anisotropy is assumed to be aligned parallel to the Y-direction; when the anisotropy factor equals 1, the fracture surface is assumed to be homogeneous [22].

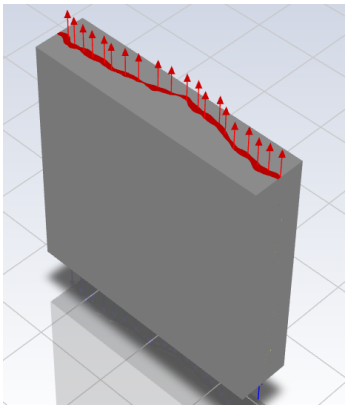


Figure 1. Geothermal fracture model.

3 NUMERICAL SIMULATIONS

The established model was imported into Fluent. The finite volume method was adopted in Fluent for computation, where the computational domain was discretized into several control volumes. Conservation equations were integrated into each volume, and flux calculations were employed to ensure physical quantity conservation. This approach is suitable for complex geometries such as fractures and guarantees local conservation [23]. Boundary conditions were set in Fluent. During the numerical simulation, the temperature of the outer rock wall was defined as a constant temperature boundary condition. The outer rock wall temperature was set to 150 °C. A constant flow rate boundary condition was applied for water injection at the fracture inlet, while a constant temperature boundary condition was set for the inlet water temperature. The water pressure at the fracture outlet was set to standard atmospheric pressure, and the fracture aperture was fixed at a constant value of 0.2 mm [24]. The flow regime was determined by calculating the velocity based on the selected injection flow rate, and then derived the Reynolds number from this velocity. The injection flow rates selected were 0.0005 kg/s, 0.001 kg/s, 0.0015 kg/s, and 0.002 kg/s. The flow velocity was calculated based on the fracture aperture, length, and the density of supercritical carbon dioxide, and the Reynolds number was subsequently determined to be approximately 100-200, indicating that the flow regime of supercritical carbon dioxide in the fracture is turbulent.

$$Re = \frac{\rho v L}{\mu} \quad (4)$$

Where ρ is the fluid density, μ is the fluid viscosity, v is the characteristic velocity of the fluid, and L is the characteristic length of the fluid.

In the general settings, the transient option was selected. The rock material was defined as "rock" in the Fluent database. The thermophysical properties of carbon dioxide were calculated using the REFPROP real gas model. The results were then compiled into a user-defined function (UDF) and imported into Fluent to replace the default ideal gas model, thereby obtaining property parameter curves for carbon dioxide [25].

This study aims to investigate the effects of different injection temperatures, injection flow rates, ambient pressures, and wall temperatures on the flow and heat transfer characteristics and the heat production rate of supercritical carbon dioxide. For studying the influence of injection temperature on the flow characteristics of supercritical CO_2, the injection temperatures were set to 15 °C, 30 °C, 45 °C, and 60 °C, with an injection flow rate of 0.0005 kg/s, a wall temperature of 150 °C, and an ambient pressure of 25 MPa. For studying the influence of ambient pressure, the ambient pressures were set to 15 MPa, 25 MPa, and 35 MPa, with an injection temperature of 15 °C, an injection flow rate of 0.0005 kg/s, and a wall temperature of 150 °C. For studying the influence of injection flow rate, the flow rates were set to 0.0005 kg/s, 0.001 kg/s, 0.0015 kg/s, and 0.002 kg/s, with an injection temperature of 20 °C, a wall temperature of 150 °C, and an ambient pressure of 25 MPa. For studying the influence of wall temperature, the wall temperatures were set to 120 °C, 160 °C, 200 °C, and 240 °C, with an injection temperature of 20 °C, an ambient pressure of 25 MPa, and an injection flow rate of 0.0005 kg/s. The transient formulation was selected for the calculations. Data were recorded at a time step interval of 5, and the iterative calculation was terminated when the temperature of supercritical carbon dioxide stabilized with no abrupt changes.

4 RESULTS ANALYSIS

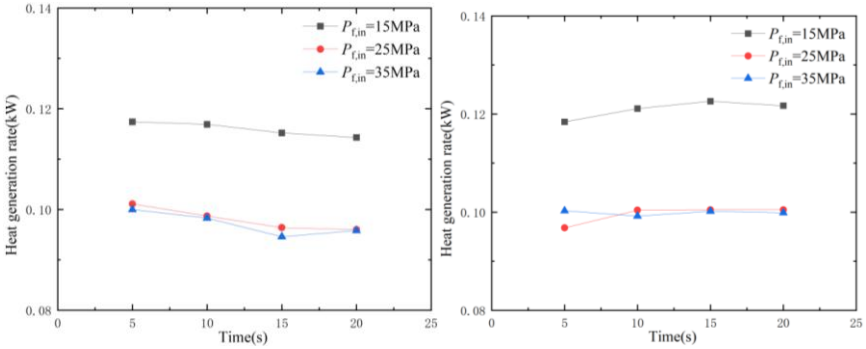
In this study, the heat production rate is closely related to multiple factors:

$$Q = q_{m,out} \cdot h_{out} - q_{m,in} \cdot h_{in} \tag{5}$$

Along the flow direction of supercritical carbon dioxide, starting from the fluid inlet cross-section, cross-sections were taken at positions of 0.005 m, 0.015 m, 0.025 m, 0.035 m, and 0.045 m. The contour plots, arranged from top to bottom, correspond to the cross-sections at 0.005 m, 0.015 m, 0.025 m, 0.035 m, and 0.045 m, respectively, with the fluid outlet located on the right side of the contour plots.

4.1 Ambient Pressure

In Figure 2, it shows that when the ambient pressure increases, the heat production rate decreases at an anisotropy factor of 1, and gradually declines over the duration of the heat transfer process. At an ambient pressure of 35 MPa, the heat production rate of hot dry rock reaches its minimum value of 0.0946 kW when the heat transfer process reaches 15 seconds. At an anisotropy factor of 1.05, the heat production rate shows no significant variation with ambient pressure. However, it can be observed that the heat production rate of hot dry rock reaches its maximum at 15 MPa ambient pressure.

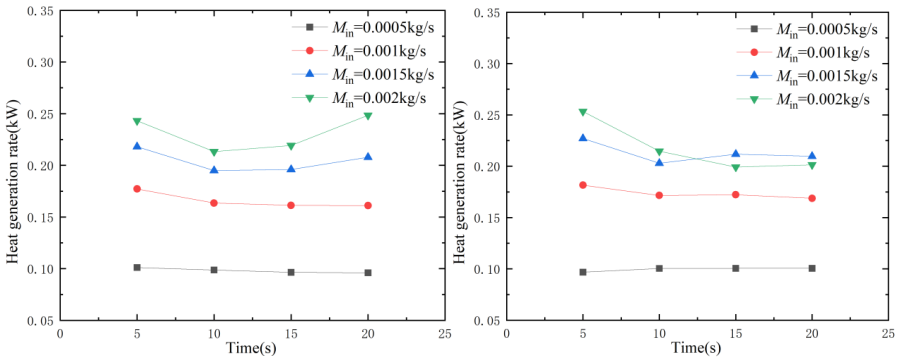


(a) *An*=1.00 (b) *An*=1.05

Figure 2. Point line graph of the variation law of heat production rate between model one and model two when the environmental pressure is different.

4.2 Injection Flow Rate

Figure 3 shows that when the injection flow rate of carbon dioxide increases, the heat production rate increases with increasing injection flow rate at an anisotropy factor of 1. Over the heat transfer process duration, the variation patterns of heat production rate differ significantly across different injection flow rates. At an injection flow rate of 0.0005 kg/s, the heat production rate remains nearly constant throughout the process. At 0.001 kg/s, it first decreases and then stabilizes. At 0.0015 kg/s and 0.002 kg/s, the heat production rate first decreases and then increases, with the former reaching a peak of 0.2181 kW at 5 seconds and the latter peaking at 0.2484 kW at 20 seconds. At an anisotropy factor of 1.05, no clear variation pattern of heat production rate with injection flow rate is observed. However, it can be noted that approximately 12 seconds into the heat transfer process, the heat production rate at 0.002 kg/s injection flow rate is higher than at 0.0015 kg/s.

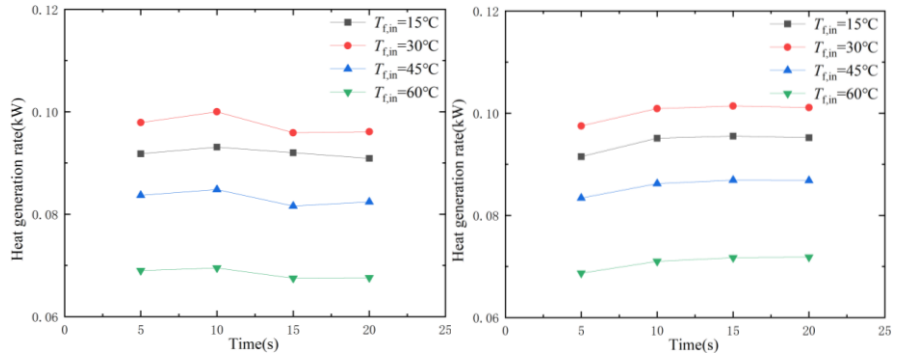


(a) *An*=1.00 (b) *An*=1.05

Figure 3. Point line graph of the variation law of heat production rate between model one and model two when the injection flow rate is different.

4.3 Injection Temperature

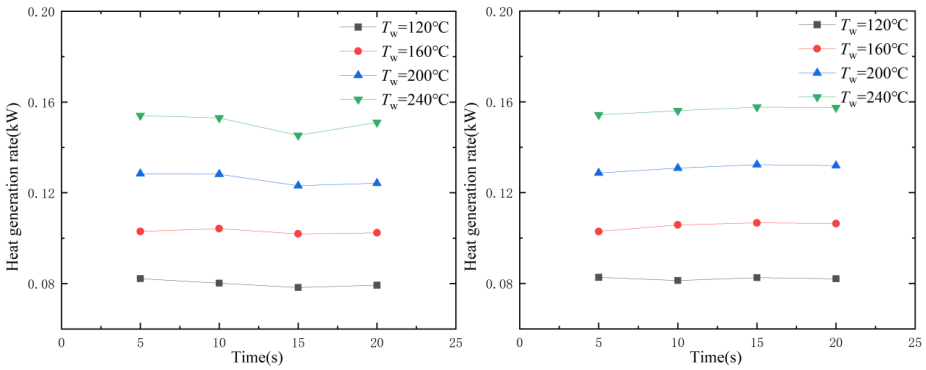
In Figure 4, it shows that as the injection temperature of carbon dioxide increases, no clear pattern is observed in the heat production rate at an anisotropy factor of 1. The highest heat production rate occurs at 30 °C, followed by 15 °C, 45 °C, and 60 °C. Over the heat transfer process duration, the variation patterns of heat production rate differ significantly across different injection temperatures. At 15 °C, the heat production rate first increases then decreases, peaking at 0.0931 kW in 10 seconds. At 30 °C, 45 °C, and 60 °C, the heat production rate first increases, then decreases, followed by slight recovery. At an anisotropy factor of 1.05, no clear pattern is observed in the heat production rate.



(a) *An*=1.00 (b) *An*=1.05

Figure 4. Point line graph of the variation law of heat production rate between model one and model two when the injection temperature is different.

4.4 Wall Temperature



(a) *An*=1.00 (b) *An*=1.05

Figure5. Point line graph of the variation law of heat production rate between model one and model two when the wall temperature is different.

Figure 5 shows that when the hot dry rock wall temperature increases, the heat production rate increases at an anisotropy factor of 1. Over the heat transfer process duration, the variation patterns of heat production rate

show little difference at wall temperatures of 120 °C, 160 °C, and 200 °C. At a wall temperature of 240 °C, the heat production rate first decreases then increases, peaking at 0.154 kW at 5 seconds and reaching a minimum of 0.1453 kW at 15 seconds. At an anisotropy factor of 1.05, the heat production rate increases with increasing hot dry rock wall temperature.

4.5 Multi-objective Optimization Design

To further optimize the fracture structure and flow parameters for both the highest heat production rate and the lowest pressure drop, a multi-objective optimization design study was conducted on flow and heat transfer in rough fractures. The flowchart of the multi-objective optimization process is shown in Figure 6.

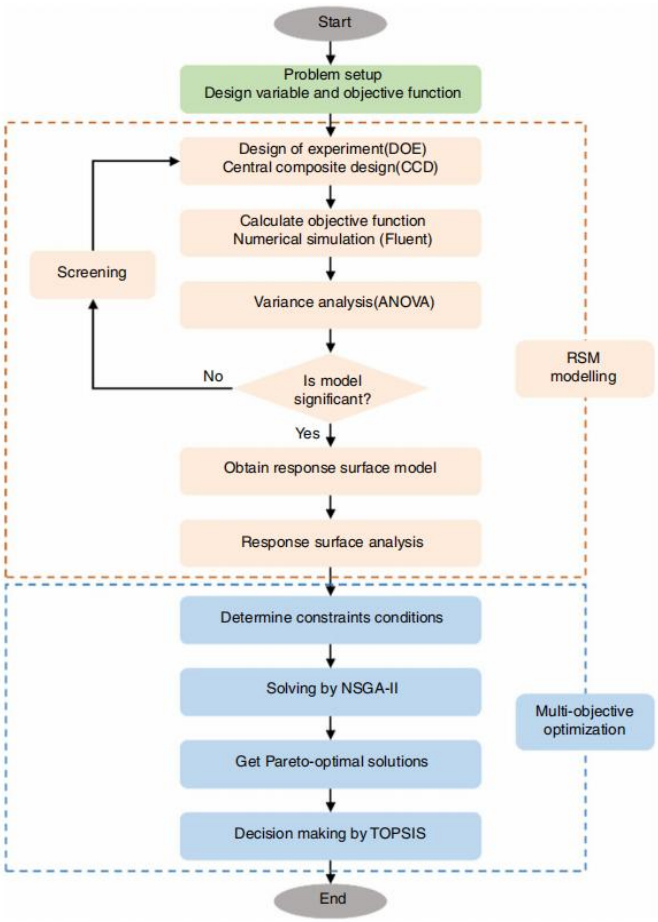


Figure 6. Multi-objective optimization process flowchart.

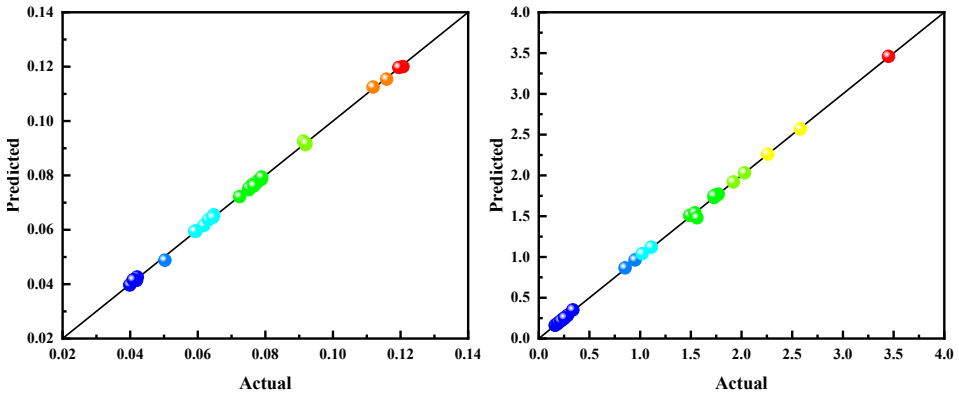
Considering that the flow and heat transfer characteristics of supercritical carbon dioxide in geothermal extraction fractures are primarily influenced by flow parameters and fracture structural parameters, and evaluating the impact of fracture roughness, this study maintains a constant aperture (0.2 mm). Therefore, four design parameters are defined for the optimization problem in this study: (1) Injection flow rate M_{in}; (2) Injection temperature $T_{f,in}$; (3) Anisotropy factor An; (4) Fractal dimension D.

Table 1. Design parameters and ranges.

No.	Design Parameter	Range		
		-1	0	1
1	Injection flow rate M_{in} (kg/s)	0.0005	0.00125	0.002
2	Injection temperature $T_{f,in}$ (°C)	15	37.5	60
3	Anisotropy factor An	1	1.05	1.1
4	Fractal dimension D	2.1	2.15	2.2

Figure 7 presents a comparison between the simulated values and the predicted values from the regression model for the heat production rate Q and the pressure drop Δp. It can be observed that the predicted values of

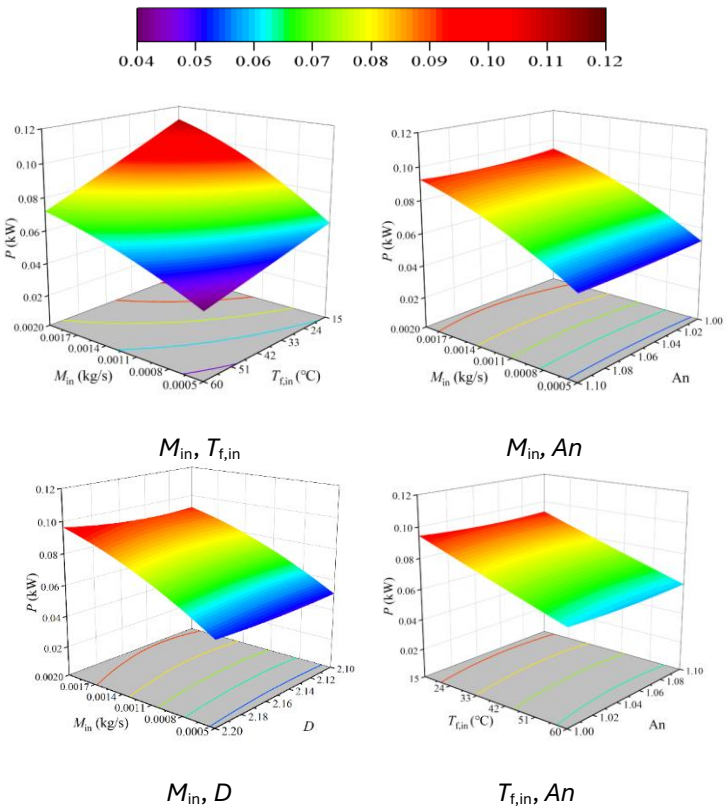
the heat production rate *Q* agree well with the actual values, with a maximum relative error of 0.63%. The predicted values of the pressure drop Δ*p* also show good agreement with the actual values, with a maximum relative error of 4.07%. Overall, the established regression model can serve as a surrogate function for calculating the relationship between the objective functions and the influencing factors.



(a) heat production rate *Q* (b) pressure drop Δ*p*

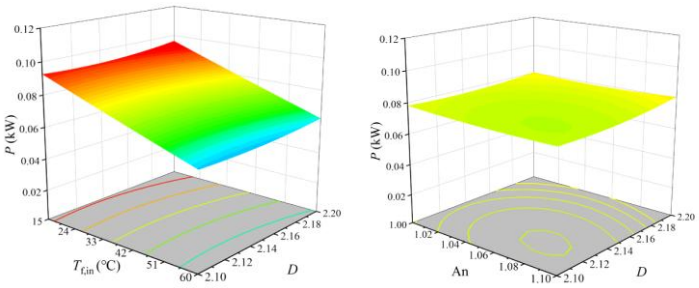
Figure 7. Comparison of actual simulation results and regression model prediction results for (a) heat production rate *Q* and (b) pressure drop Δ*p*.

Figure 8 presents the response surface results for the heat production rate Q. It can be observed that Q is primarily influenced by injection flow rate Min and injection temperature Tf,in, gradually reaching its maximum value with increasing injection flow rate and injection temperature. The anisotropy factor An and fractal dimension D have relatively minor effects on Q, but when An=1.08 and D=2.13, the corresponding heat production rate reaches a minimum value. Figure 9 shows the response surface results for the pressure drop Δp. It can be seen that Δp is mainly affected by the injection flow rate Min, gradually reaching its maximum value with an increasing injection flow rate. Furthermore, as the flow velocity increases, the influences of injection temperature Tf,in, anisotropy factor An, and fractal dimension D on Δp become progressively more significant. When An=1.04 and D=2.16, the corresponding pressure drop reaches a maximum value.



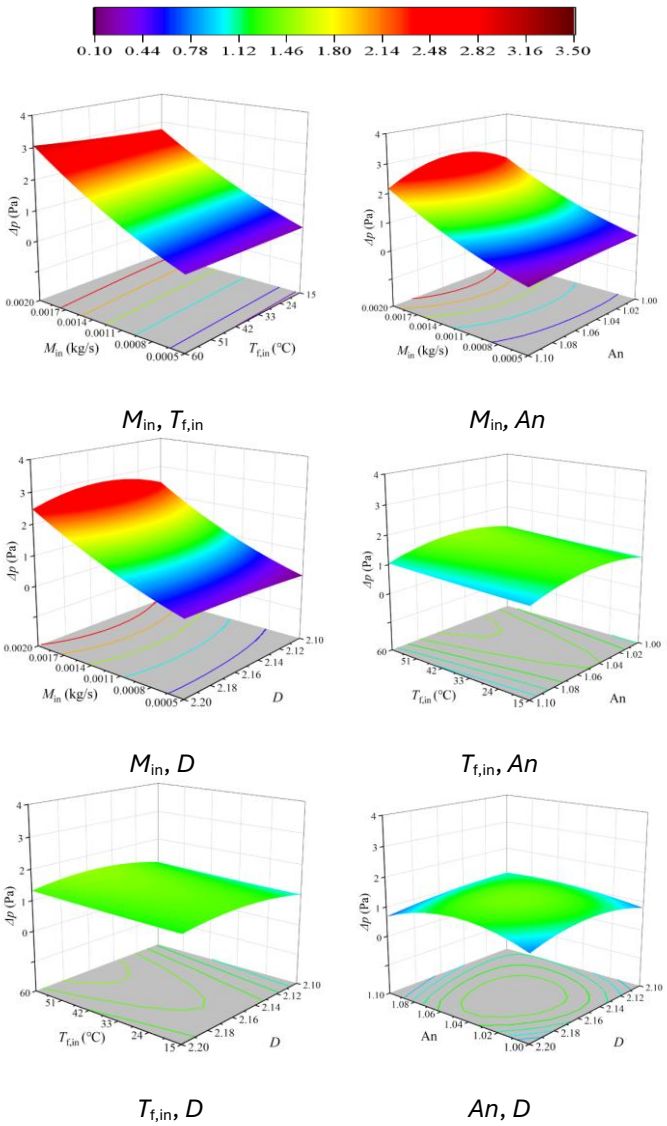
M_{in}, $T_{f,in}$ M_{in}, *An*

M_{in}, *D* $T_{f,in}$, *An*



$T_{f,in}$, D An, D

Figure 8. Response surface of heat production rate Q.



M_{in}, $T_{f,in}$ M_{in}, An

M_{in}, D $T_{f,in}$, An

$T_{f,in}$, D An, D

Figure 9. Response surface of pressure drop Δp.

With the objectives of maximizing the heat production rate Q and minimizing the pressure drop Δp, the established regression model is employed as a surrogate function. The NSGA-II algorithm was applied to conduct a multi-objective optimization design. In Figure 10, the red dots represent the Pareto optimal solutions obtained through the optimization design, showing the distribution of solutions that maximize heat production rate while minimizing pressure drop. The pink pentagram points indicate ideal points with maximum heat production rate and minimum pressure drop, which do not exist in practice. Considering engineering application requirements, the point with the smallest dimensionless distance to the ideal point was selected as the recommended solution based on the TOPSIS method. The blue pentagram point in the figure represents the closest point to the ideal point, and its corresponding structural and flow parameters are recommended for practical engineering applications.

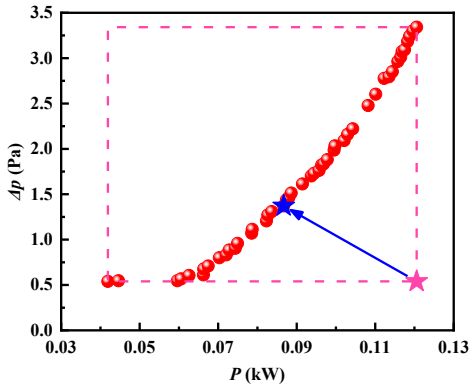


Figure 10. Pareto optimal solutions.

5 CONCLUSIONS

This study successfully investigated the effects of different ambient pressures, injection flow rates, injection temperatures, and wall temperatures on the flow and heat transfer characteristics as well as the heat production rate of supercritical carbon dioxide in rough fractures.

When the anisotropy factor is 1, the heat production rate decreases with increasing ambient pressure, increases with rising injection flow rate, and rises with an increase in hot dry rock wall temperature. In contrast, when the anisotropy factor is 1.05, the heat production rate increases with increasing hot dry rock wall temperature, while its variations with ambient pressure and injection flow rate exhibit no clear patterns. Notably, changes in injection temperature do not yield a distinct correlation with the heat production rate in either case. The anisotropy factor of fractures significantly modulates the pressure distribution, flow velocity, and heat production rate of supercritical carbon dioxide by altering wall roughness and flow paths. This results in distinctly different local flow and heat transfer characteristics, as well as variations in heat production rate, under identical conditions for models with different anisotropy factors.

A multi-objective optimization study was conducted with the objectives of maximizing heat production rate and minimizing pressure drop, resulting in a Pareto frontier representing optimal trade-offs. Based on the minimum dimensionless distance to the ideal point of maximum heat production rate and minimum pressure drop, a recommended solution was obtained with M_{in}=0.000983 kg/s, $T_{f,in}$=15.0753 °C, *An*=1.099725, and *D*=2.199909. This configuration achieves a heat production rate of 0.086703 kW while maintaining a fracture pressure drop of only 1.371932 Pa.

Acknowledgements

The authors would like to acknowledge the NSFC project (Grant No. 52192620; Grant No. 52125401; Grant No. 52574061) and the Fundamental Research Fund of the University (2462024YJRC010).

REFERENCES

[1] Zhang, H.J.: Global Standards Could Promote New Energy Industries' Rapid Development, *Standard Living*, 3, (2010), 62-69.

[2] Li, N.N., Tao, C., Kong, Y.L., et al: Status and research progress of geothermal power generation development and utilization, *Thermal Power Generation*, 53, 6, (2024), 1-11.

[3] Jiang, Y.R., Ding, H.R., and Jiang, N.: Research and Development Situation Analysis in Sub-fields Based on Patent Bibliometric: Taking the Development of Dry Hot Rock Enhanced Geothermal Systems in the Clean Energy Industry as an Example, *Science and Technology Management Research*, 45, 5, (2025), 149-160.

[4] Cui, X.Y.: Study on Heat Transfer Characteristics of Strongly Variable-Properties Fluids and Optimization Method of High Efficient Heat Exchanger, *University of Chinese Academy of Sciences* (Institute of Engineering Thermophysics, Chinese Academy of Sciences), 2020.

[5] Peng, D., Robinson, D.B.: A new two-constant equation of state, *Industrial & Engineering Chemistry Fundamentals*, 15, 1, (1976), 59-64.

[6] Span, R., and Wagner, W.: A new equation of state for carbon dioxide covering the fluid region from the triple-point temperature to 1100 K at pressures up to 800 MPa, *Journal of physical and chemical reference data*, 25, 6, (1996), 1509-1596.

[7] Magliocco, M., Kneafsey, T.J., Pruess, K., et al: Laboratory experimental study of heat extraction from porous media by means of CO_2, *36th Workshop on Geothermal Reservoir Engineering*, (2011).

[8] Zhang, L., Xu, R.N., and Jiang, P.X.: Experimental Research on Convection Heat Transfer of Supercritical CO2 in the Smooth Fracture of Granite Rock, *Journal of Engineering Thermophysics*, 37, 7, (2016), 1500-1505.

[9] Gong, L., Han, D.X., Chen, Z., et al: Research status and development trend of key technologies for an enhanced geothermal system, *Natural Gas Industry*, 42, 7, (2022), 135-159.

[10] Han, D.X., Zhang, W.T., Jiao, K.T., et al: Analysis of thermal-hydraulic-mechanical-chemical coupling for EGS based on embedded discrete fracture model, *Natural Gas Industry*, 43, 7, (2023), 126-138.

[11] Zhang, F.Z., Jiang, P.X., and Xu, R.N.: System thermodynamic performance comparison of CO_2-EGS and water-EGS systems, *Applied Thermal Engineering*, 61, 2, (2013), 236- 244.

[12] Brown, D.: A hot dry rock geothermal energy concept utilizing supercritical CO_2 instead of water, *Twenty-Fifth Workshop on Geothermal Resevoir Engineering*, (2000).

[13] Zhou, C., Remoroza, I.A., Shah, K., et al: Experimental study of static and dynamic interactions between supercritical CO_2/water and Australian granites, *Geothermics*, 64, (2016), 246-261.

[14] Li, S.: Numerical Study on Seepage-Heat Transfer Characteristics of Supercritical CO2 in the Fractured Reservoir, *Tianjin University*, (2019).

[15] Xu, Z.H., Du, B., and Li, D.D.: Numerical Simulation Study on the Phase Distribution Characteristics of CO2 Fracturing Fluid inside Cracks, *China Resources Comprehensive Utilization*, 42, 4, (2024), 41-43.

[16] Jiang, H.Y., Cao, Y.L., and Liu, L.: Evaluation of deep granitic geothermal resource potential based on discrete fracture network model: Taken as an example of the 3003.17m geothermal exploration well in Wendeng granite body in Shandong Province, *Geology in China*, 50, 3, (2023), 534-547.

[17] Wang, S., Javadpour, F., and Feng, Q.: Molecular dynamics simulations of oil transport through inorganic nanopores in shale, *Fuel*, 171, (2016), 74-86.

[18] Jiang, C., Ouyang, J., Liu, Q., et al: Studying the viscosity of methane fluid for different resolution levels models using Poiseuille flow in a nano-channel, *Microfluidics and Nanofluidics*, 20, 12, (2016), 157.

[19] Yao, J., Zhang, Xu., Sun, Z.X., et al: Numerical simulation of the heat extraction in 3D-EGS with thermal-hydraulicmechanical coupling method based on discrete fractures model, *Geothermics*, 74, (2018), 19-34.

[20] Zhang, L.: Research on Convection Heat Transfer of Supercritical Pressure CO2 in Rock Fracture and Porous Media, *Tsinghua University*, (2017).

[21] Lerbekmo, J.F.: A tool for obtaining oriented samples of weakly to moderately indurated sedimentary rocks for paleomagnetic measurements. *Sedimentary Geology*, 66, 3-4, (1990), 295-299.

[22] Li, J.W., and Ye, L.: Investigations of Water Flow Behaviors Induced by Local Temperature Variations through a Single Rough Fracture for the Enhanced Geothermal Systems, *Journal of Thermal Science*, 33, 3, (2024), 1055-1064.

[23] Yang, J.L., Li, J., Chen, X.W., et al: Practice and application on digital twin Pearl River construction, *China Water Resources*, 8, (2025): 39-46.

[24] Liu, W.T.: Research on Flow and Heat Transfer of Water and Supercritical CO2 in High-temperature Granite Fracture, *Chengdu University of Technology*, (2022).

[25] Su, X.P.: Flow Behavior in Granite Fractures and Mechanism of Hydraulic Fracture Propagation, *Chongqing University*, (2020).